Optics Communications 371 (2016) 132–137

Contents lists available at ScienceDirect

Optics Communications

journal homepage: www.elsevier.com/locate/optcom

Refractive index and temperature nanosensor with plasmonic waveguide system

Yan Kong*, Peng Qiu, Qi Wei, Wei Quan, Shouyu Wang, Weiying Qian

School of Science, Jiangsu Provincial Research Center of Light Industrial Optoelectronic Engineering and Technology, Jiangnan University, Wuxi 214122, China

ARTICLE INFO

Article history:
Received 25 January 2016
Received in revised form
23 March 2016
Accepted 25 March 2016

Keywords:
Surface plasmon polaritons
Sensor
Refractive index
Temperature

ABSTRACT

A surface plasmon polariton sensor consisting of two metal–insulator–metal waveguides and a transverse rectangular resonator is proposed. Both refractive index and temperature sensing characteristics are analyzed by investigating the transmission spectra which demonstrates that the transmission peak wavelength shifting satisfies linear relation with environmental refractive index and temperature, respectively. The proposed design provides high refractive index and temperature sensitivity as 3.38×10^6%/RIU and 82%/K estimated by integrated response of the sensor, and owns the potentials for high-throughput array sensing. It is believed that the nanoscale sensor can be applied in spot detection for high speed multi-parameter sensing and accurate measurements.

1. Introduction

Continuous improvements in nanofabrication change projections about the role that metals can play in the development of new optical devices [1]. Surface plasmon polaritons (SPPs) are the electromagnetic surface waves coupled to coherent charge oscillations at the metal-dielectric interface, and the excitation of SPPs can generate large field enhancements within nanoscale volumes [2]. The unprecedented concentration of light and strong interactions between light and matter in nanostructures open up new opportunities in biological and chemical sensing, fluorescence, Raman scattering, lithography, and photovoltaics, etc. [3]. Among these applications, sensing is a hotspot: various optical sensors have been demonstrated [4–6], in which thin metal films were deposited on integrated optical waveguides as platforms for the attachment of sensing films. Most of these integrated surface plasmon resonance sensors were made from dielectric materials with low refractive index contrast. However, they were unsuitable for lab-on-chip applications because the size of these bulk optical components was too large to be miniaturized. Compared to other sensors, SPP sensors offer promising potentials for miniaturization, low cost-production and massive multiplexing capacity [7–10]. As most previously reported SPP sensors often focused on single-channel spectral interrogation with their demonstrated superior performance [11–13], it is worth noting that sensing scheme requires the multi-channel structure to detect diversified binding events sequentially [14,15] rather than simultaneously, with the help of image sensors for simultaneously supplying the spatial and temporal information [10,16,17]. The developing trend claims that the SPP sensors should own not only simple structure and miniaturization potentiality, but also extremely high sensitivity and multi-channel detecting capacity.

To satisfy demands of future sensor requirements, in this paper, we propose a SPP sensor consisting of two metal–insulator–metal (MIM) waveguides coupled by transverse rectangular resonator which can realize both environmental refractive index (*RI*) and temperature sensing. Both environmental *RI* and temperature sensing sensitivities are studied according to theoretical analysis and numerical simulation which show that the proposed design is capable of obtaining quantitative *RI* and temperature information with high sensitivity. Compared to previous sensors [18–20], it not only owns rather high sensitivity, but also simple and compact structure. Thus, it can be easily fabricated, and multiple channels can be integrated as sensing array for high-throughput detection. Besides, multiple structures can be integrated as sensing array for high-throughput detection. Finally, to understand the dependence of sensing performance on sensor construction, the structural parameters of the sensor are quantitatively analyzed which can be a reference for sensor optimization. It is believed that the proposed design can be applied in spot detection in the future for high speed multi-parameter sensing and accurate measurements.

2. Structure design and theoretical analysis

The designed sensor array is shown in Fig. 1. The unit cell of silver fabricated SPP sensor is composed of two MIM waveguides

* Corresponding author.
E-mail address: ykong80@163.com (Y. Kong).

http://dx.doi.org/10.1016/j.optcom.2016.03.072
0030-4018/

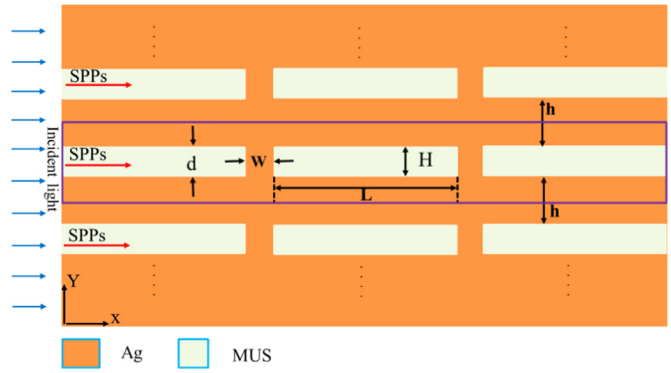

Fig. 1. Scheme of periodic MIM waveguide based sensing array. The orange and white areas indicate silver and MUS, respectively. *d* is the width of slit, *w* is the coupling length between the waveguides and the transverse rectangular, *L* and *H* are the length and the height of the transverse rectangular, *h* is the thickness of metal between two waveguide. The arrow shows the direction of the incident light. (For interpretation of the references to color in this figure legend, the reader is referred to the web version of this article.)

and a transverse rectangular resonator as shown in the central rectangular. The materials under sensing (MUS) can be filled up in the sensor for detection.

The dispersion relation of the fundamental TM mode in the MIM waveguide is given by Eq. (1) [21,22]

$$\varepsilon_{in}k_{z2} + \varepsilon_m k_{z1}\coth(-ik_{z1}d/2) = 0 \tag{1}$$

k_{z1} and k_{z2} are defined by momentum conservations.

$$k_{z1}^2 = \varepsilon_{in}k_0^2 - \beta^2 \tag{2}$$

$$k_{z2}^2 = \varepsilon_m k_0^2 - \beta^2 \tag{3}$$

where ε_{in} and ε_m are permittivities of insulator and metal, respectively, β is the propagation constant of SPPs and $k_0=2\pi/\lambda$ is the free-space wave vector.

The frequency-dependent complex dielectric function of silver is characterized by Drude model in Eq. (4).

$$\epsilon_m(\omega) = 1-\frac{\omega_p^2}{\omega(\omega + i\omega_c)} \tag{4}$$

ω_p denotes the temperature-dependent plasma frequency given by Eq. (5) [20].

$$\omega_p(T) = \omega_p(T_0)\exp\left\{-\frac{1}{2}\int_{T_0}^{T}\alpha_v(T)dT\right\} \tag{5}$$

where $\omega_p(T_0)=\sqrt{4\pi Ne^2/m^*}$, m^* and N represent the effective mass and the density of the conduction electrons at room temperature T_0, respectively. $\alpha_V(T)$ is the volumetric thermal expansion coefficient of the metal varying with temperature [21]. ω_c represents the temperature-dependent collision frequency shown as Eq. (6) [23].

$$\omega_c = \frac{1}{6}\pi^4\frac{\Gamma\Delta}{h_pE_F}\left[(k_BT)^2 + \left(\frac{h_p\omega}{4\pi^2}\right)^2\right] + \omega_0\left[\frac{2}{5} + 4\left(\frac{T}{T_D}\right)^5\int_0^{\frac{T_D}{T}}\frac{z^4}{e^z-1}dz\right] \tag{6}$$

Γ is a constant giving the average over the Fermi surface of the scattering probability, and Δ represents the fractional Umklapp scattering. k_B, h_p and T_D are Boltzmann constant, Plank constant, Debye temperature, respectively, and ω_0 is a constant to each metal.

As temperature influences the thickness of metal film, the variation of its thermal expansion should be considered, the corresponding expression of film thickness h_1 is according to Eq. (7) [23].

$$h_1(T) = h_{10}\exp\left\{\int_{T_0}^{T}\alpha_L(T)dT\right\} \tag{7}$$

where h_{10} is the thickness of metal film at room temperature. $\alpha_L(T)$ is the linear thermal expansion coefficient of bulk metals, expressed as Eq. (8) [24].

$$\alpha_L(T) = \frac{\alpha_V(T)}{3}\frac{1+\mu}{1-\mu} \tag{8}$$

μ is the Poisson number of metal. The values of the metal parameters used in our simulations are all taken from Refs. [23,24].

The real part of the propagation constant β can be used to evaluate the effective refractive index as $n_{eff}=Re(\beta/k_0)$. The dependence of n_{eff} of MIM waveguide for SPPs on environmental *RI* and incident wavelengths is calculated as shown in Fig. 2(a) when the temperature is at 300 K, $\omega_p=1.37\times10^{16}$ rad/s and $\omega_c=4.84\times10^{13}$ rad/s. Moreover, in this model, $d=50$ nm, $W=10$ nm, $L=900$ nm. From Fig. 2(a), n_{eff} is almost linear with *RI* at given wavelengths. Besides, the temperature influence is also considered here: Fig. 2(b) and (c) shows the variations of dielectric function and thickness of silver with temperature, respectively. These curves indicate that both real and imaginary parts of the silver-dielectric function, as well as the thickness of silver, grow with temperature increasing.

The rectangular resonator structure behaves as a standing-wave resonator supporting a resonant mode at the frequency of ω_0 corresponding to the resonant wavelength λ_0. Using the temporal coupled-mode theory, the transmission of this structure can be described as Eq. (9) [25–27].

$$T = \frac{\Gamma^2}{(\Delta\omega)^2 + (\Gamma_0+\Gamma)^2} \tag{9}$$

where $\Delta\omega=\omega-\omega_0$, $\Gamma_0=1/\tau_0$, $\Gamma=1/\tau_-+1/\tau_+$, and $1/\tau_0$ is the decay rate due to the intrinsic loss of SPPs, $1/\tau_-$ and $1/\tau_+$ are the power coupling rates of decay into the bus and the receive waveguides, respectively, and here, $1/\tau_-=1/\tau_+$. $\Delta\omega_{FWHM}$ can be calculated from the rectangular cavity parameters by equating the right hand side of Eq. (9) to half maximum, $\Delta\omega_{FWHM}=2(\Gamma_0+\Gamma)$.

At the resonant wavelength λ_0, the incident power achieves a peak in the transmission spectra according to the resonant condition:

$$\Delta\varphi = 4\pi\, Re(n_{eff})L/\lambda_0 + 2\phi = 2m\pi \tag{10}$$

where $\Delta\varphi$ is the round-trip phase-shift, Φ is the phase shift of a beam reflected at the end of the resonator, and m is an integer. According to Eq. (10), the resonant wavelength can be described as

$$\lambda_0 = 2Re(n_{eff})L/(m-\phi/\pi) \tag{11}$$

With the resonant wavelength, both environmental *RI* and temperature can be detected as shown in the following sections.

3. Results and discussions

The transmission spectra and the field distributions of the SPPs are shown in Fig. 3. Here, no material is filled in this structure except air. In Fig. 3(a), there are four transmission peaks appearing at the resonant wavelengths of 1323 nm, 885 nm, 667 nm and 538 nm, corresponding to the peak A, B, C and D with transmission rates